Zhang, H., et al., 2021, Spatially variable provenance of the Chinese Loess Plateau: Geology, v. 49, https://doi.org/10.1130/G48867.1

Supplementary Information for the paper

Spatially variable provenance of the Chinese Loess Plateau

Haobo Zhang[1], Junsheng Nie[1, 2*], Xiangjun Liu[3*], Alex Pullen[4], Guoqiang Li[1], Wenbin Peng[5], Hanzhi Zhang[6]

[1]*Key Laboratory of Western China's Environment Systems (Ministry of Education), College of Earth and Environmental Sciences, Lanzhou University, Lanzhou 730000, China.*

[2]*CAS Center for Excellence in Tibetan Plateau Earth Sciences, Chinese Academy of Sciences (CAS), Beijing 100101, China.*

[3]*College of Geography and Environmental Science, Northwest Normal University, Lanzhou 730070, China.*

[4]*Department of Environmental Engineering and Earth Sciences, Clemson University, Clemson, South Carolina 29634, USA.*

[5]*School of Tourism and Resource Environment, Zaozhuang University, Zaozhuang 277160, China.*

[6]*School of Geography and Ocean Science, Nanjing University, Nanjing 210023, China.*

**Corresponding author. Email: jnie@lzu.edu.cn; x-jliu@foxmail.com*

MATERIALS AND METHODS

We report detrital zircon U-Pb ages from two loess sites for the first time: Ledu and Jiaxian (Fig. 1). The Ledu site is in the western CLP (36°25′30.569″ N, 102°34′36.16″ E). This section is 36.2 m long and its age model is based on high resolution luminescence dating(Li et al., 2020). Detrital zircon samples were taken at 0.55, 1.5, 8.2, 12.9, 17.4, 27.55, 32.55 m, corresponding to 1.3, 14.18, 25.53, 34.26, 49.78, 73.74 and 89.69 ka. The Jiaxian site (38°16′25″ N, 110°5′25″ E) is at the northeastern CLP and its age model (ca. 8.3–2.2 Ma) was established based on magnetostratigraphy(Qiang et al., 2001). We collected one early Pleistocene loess sample (ca. 2.4 Ma) from the upper Jiaxian section. We also collected one new sample from modern fluvial sand of the Huangshui River, which is close to the Ledu site (Fig. 1) for comparison. The description, sample name and original sample ID used in this study are provided in supplementary Table S1.

All new zircon U-Pb ages were measured at the laboratory of Earth Surface Process and Environment at the Nanjing University except the sample from Jiaxian, which was measured at the Arizona LaserChron Center at the University of Arizona. The analytical methods for the samples analyzed at Nanjing University followed Zhang et al. (2018), whereas the sample analyzed at the University of Arizona followed Pullen et al. (2014); Pullen et al. (2018) and we briefly describe the procedure here. For the Laboratory in the Nanjing University, the analytical instruments are a New Wave 193-nm laser ablation system and Agilent 7700x inductively coupled plasma mass spectrometry (ICP-MS). The laser beam diameter was set to 25 μm, with a 10-Hz repetition rate and energy of 2-3 J/cm^2. Zircon 91500(Wiedenbeck et al., 1995), GJ-1(Jackson et al., 2004) and NIST 610(Pearce et al., 1997) were used as the reference material. For the Arizona laboratory, the analytical instruments are Teledyne Photon Machines G2 solid state ArF excimer laser ablation system coupled to a Thermo Fisher Scientific ELEMENT 2 single collector inductively coupled plasma mass spectrometer. The laser beam diameter was set to 12 μm, with a 7-Hz repetition rate and energy of 10.16 J/cm^2. Zircon FC-1(Black et al., 2003), R33(Black et al., 2004) and SL(Gehrels et al., 2008) were used as the reference material.

Common Pb was corrected following the method of Andersen (2002) for samples measured at Nanjing University. The treatment of discordant, reverse discordant, and high-error analyses was the same for all new data. The uncertainties are reported at the 1σ level, the "best age" for each analysis used in plotting and interpretations was from $^{206}Pb/^{238}U$ for <1000 Ma and from $^{206}Pb/^{207}Pb$ for >1000 Ma ages. For ages younger than 1000 Ma, the discordance was defined as $(^{207}Pb/^{235}U-^{206}Pb/^{238}U)/^{207}Pb/^{235}U*100$; for ages older than 1000 Ma, the discordance was defined as $(^{207}Pb/^{206}Pb-^{206}Pb/^{238}U)/^{207}Pb/^{206}Pb*100$. Analyses with >15% discordance and with >10% reverse discordance were not included, same as our previous studies(Nie et al., 2015; Nie et al., 2018).

In order to constrain the potential sources and relative contribution to Loess-Paleosol sequence, we used the non-matrix multi-dimensional scaling (MDS) statistical technique(Vermeesch, 2013; Saylor et al., 2018) and the detrital zircon DZ-Mix model(Sundell and Saylor, 2017) to help analysis. Non-matrix MDS technique is based on Kuiper or Kolmogorov-Smirnov statistical method and calculates MDS map distance between two points against the corresponding calculated dissimilarity, Kuiper statistical is more sensitive in the tails of distributions than previously used Kolmogorov-Smirnov statistic(Kuiper, 1960; Vermeesch, 2018). DZ-Mix model is based on the inverse Monte Carlo method to determine mixing proportions of source sample contributions. We also show the zircon U-Pb data in probability density plots (PDP)(Brandon, 1996), kernel density estimation (KDE)(Vermeesch, 2012), and histogram diagrams for visual comparison, the optimal kernel bandwidth of each sample are calculated from Botev et al. (2010).

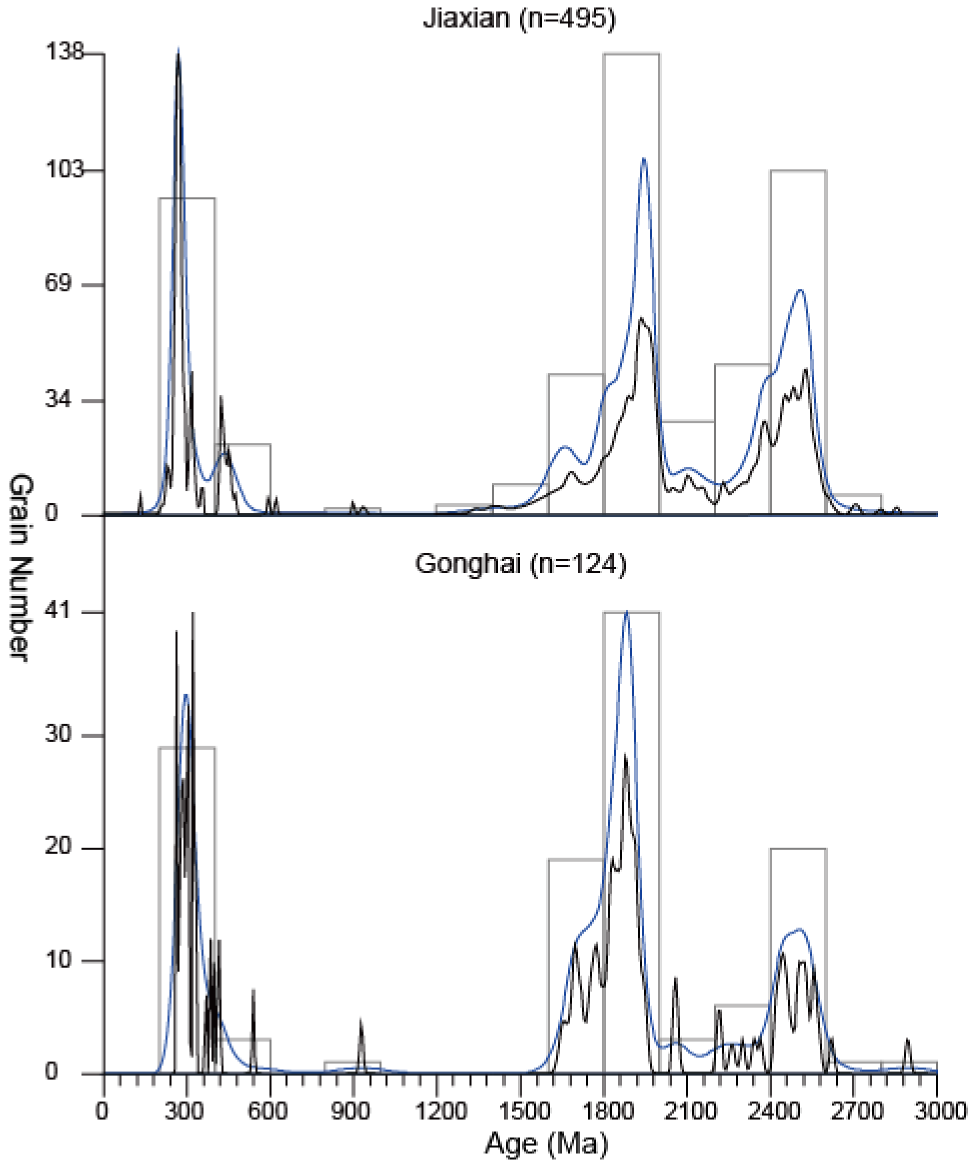

Figure S1. Visual comparison of detrital zircon U-Pb ages between Jiaxian and Gonghai. The black and blue lines are normalized probability density plots (PDP) and Kernel Density Estimation plots (KDE), respectively. The open rectangles are age histograms. The laser beam used in Jiaxian and Gonghai is 12 μm and 30 μm, respectively.

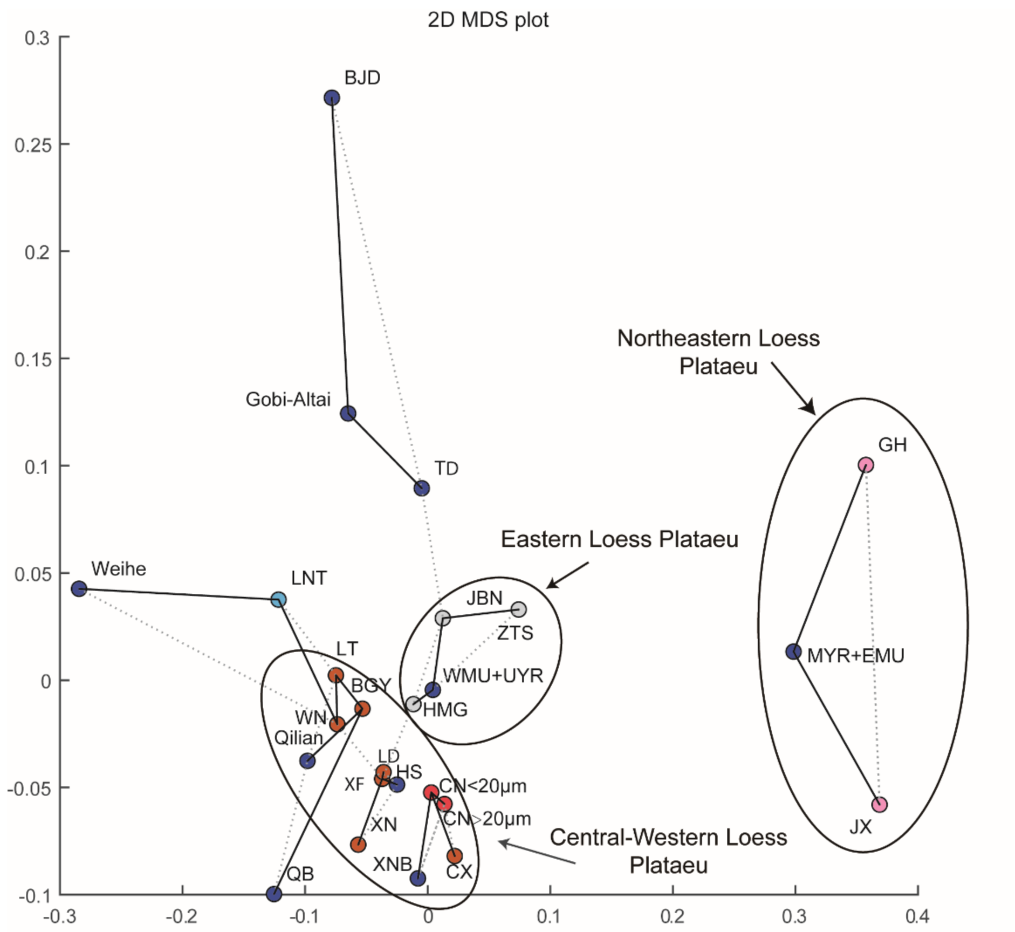

Figure S2. Non-metric multi-dimensional scaling (MDS) plot of zircon U-Pb age data of the Quaternary loess sequences on the Loess Plateau and comparison with potential sources. Brown, gray, pink, and red dots represent central-western, eastern, northeastern CLP samples, and sieved grain size samples in Chaona site (Nie et al., 2018), respectively. Dark blue dots are potential sources samples. Solid lines mark the closest neighbors and dashed lines the second closest neighbors. The three black ovals depict the clustered samples. We note that for Chana site, zircons less than 20 μm (represented by CN<20μm) have similar age pattern as zircons larger than 20 μm (represented by CN>20μm). This pattern demonstrate that grain size effect is minimal when compared with spatially variable provenance.

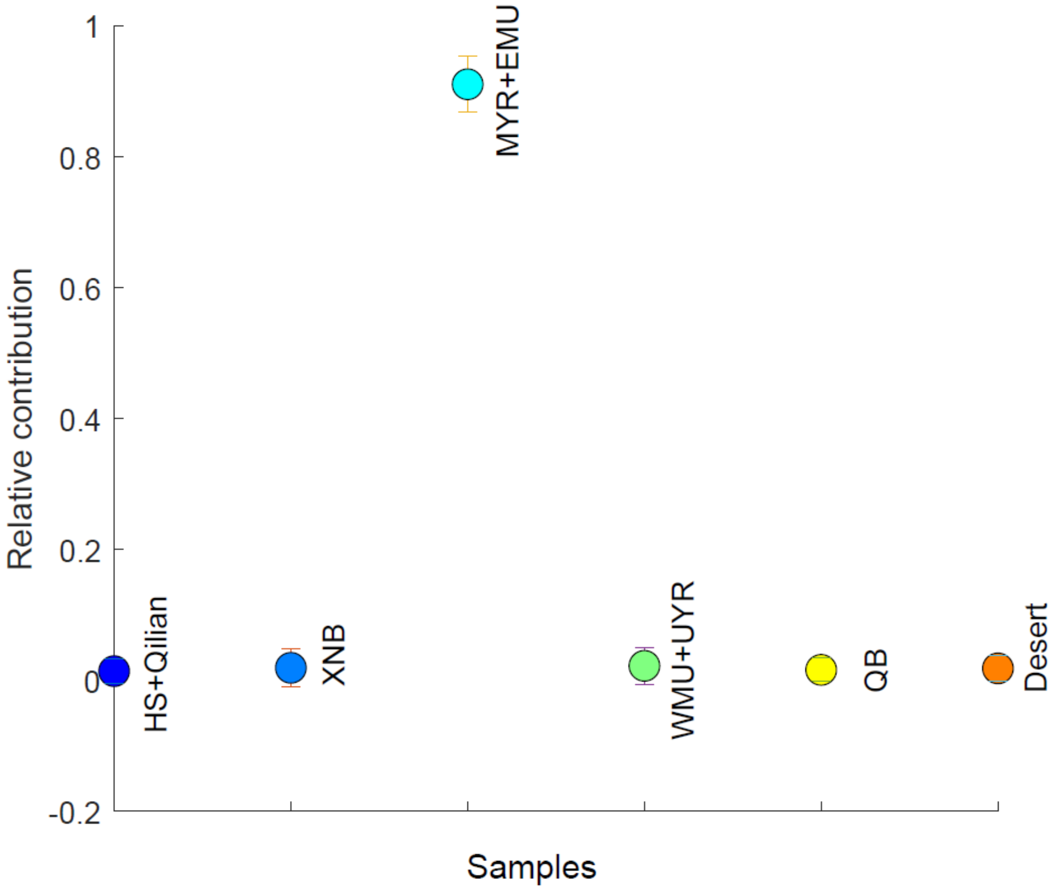

Figure S3. The relative contribution of each potential sources to northeastern CLP. HS+Qilian – Huangshui River sediment and Qilian Shan Piedmont sediment; XNB – Xining Basin sediment; EMU+MYR – Eastern Mu Us desert and Middle Yellow River sediment; WMU+UYR – Western Mu Us desert and Upper Yellow River sediment; QB – Qaidam Basin sediment; Desert – Tengger desert, Badain Jaran desert and Gobi-Altay sediment.

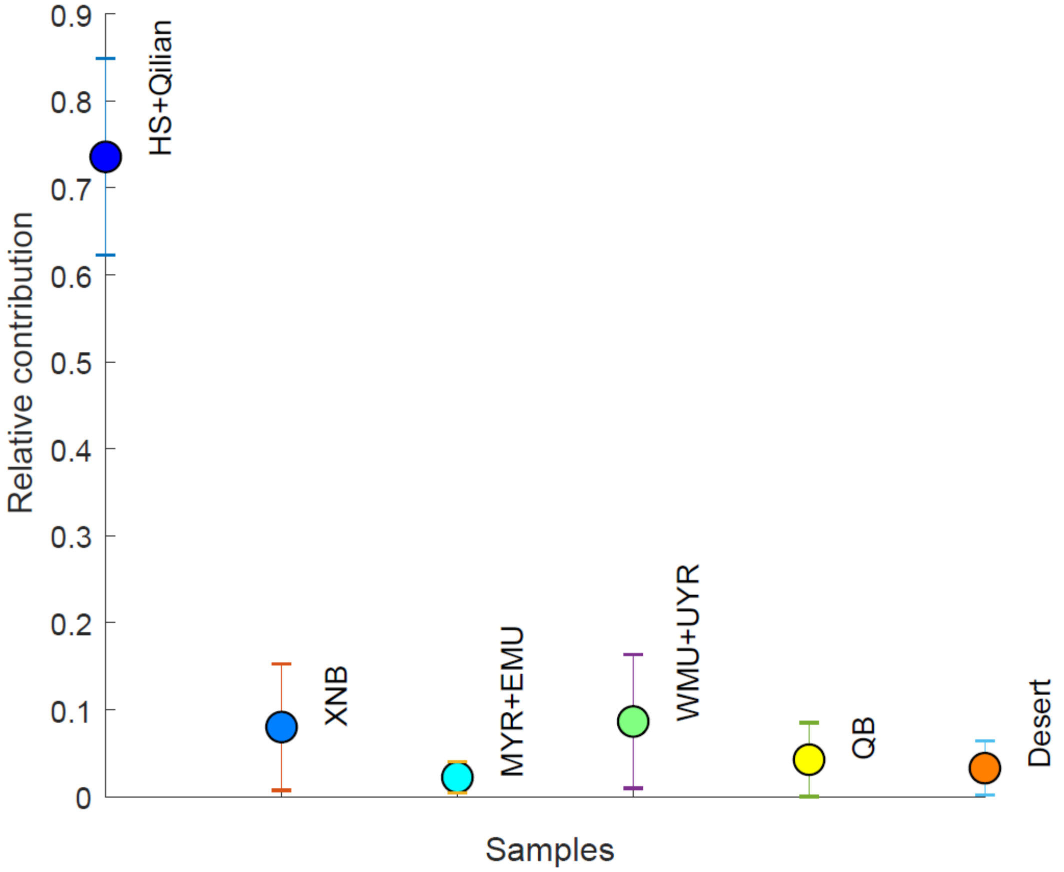

Figure S4. The relative contribution of each potential sources to central-western CLP. HS+Qilian – Huangshui River sediment and Qilian Shan Piedmont sediment; XNB – Xining Basin sediment; EMU+MYR – Eastern Mu Us desert and Middle Yellow River sediment; WMU+UYR – Western Mu Us desert and Upper Yellow River sediment; QB – Qaidam Basin sediment; Desert – Tengger desert, Badain Jaran desert and Gobi-Altay sediment.

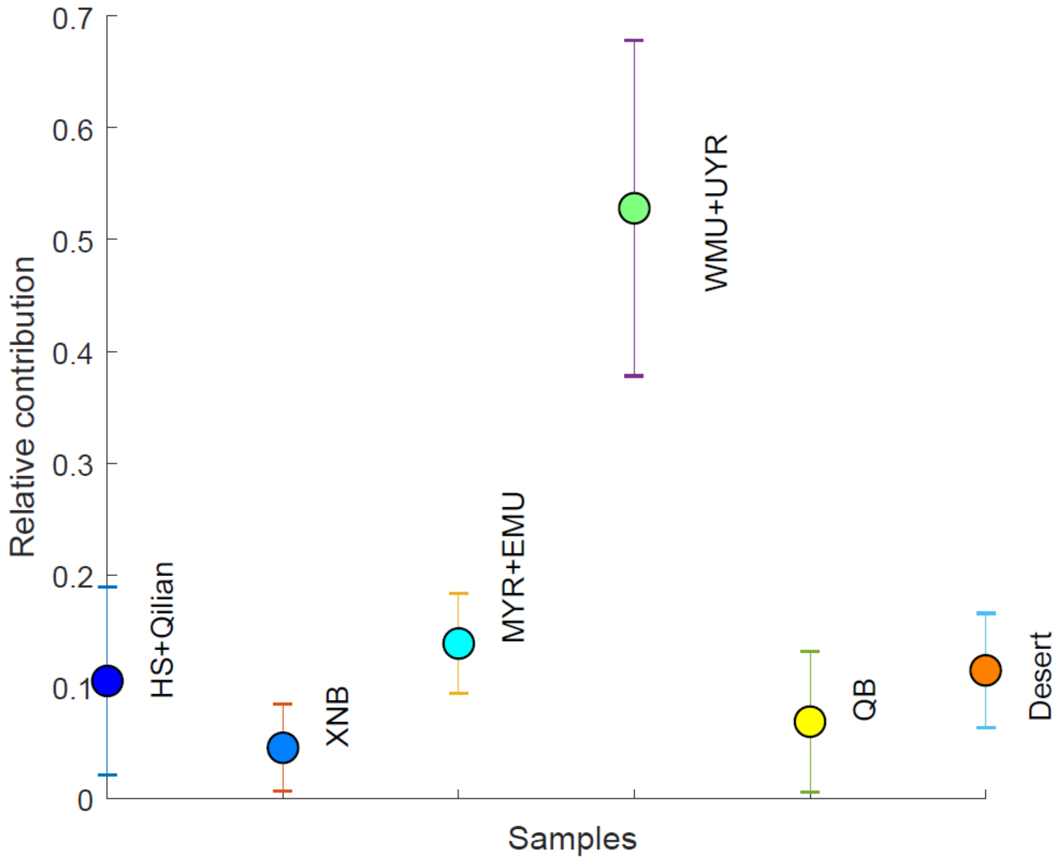

Figure S5. The relative contribution of each potential sources to eastern CLP.

HS+Qilian – Huangshui River sediment and Qilian Shan Piedmont sediment; XNB – Xining Basin sediment; EMU+MYR – Eastern Mu Us desert and Middle Yellow River sediment; WMU+UYR – Western Mu Us desert and Upper Yellow River sediment; QB – Qaidam Basin sediment; Desert – Tengger desert, Badain Jaran desert and Gobi-Altay sediment.

TABLE S1: LOCATION OF SAMPLES USED FOR ZIRCON U-PB PROVENANCE ANALYSES IN THIS STUDY. REFERENCES ARE SHOWN FOR PREVIOUSLY PUBLISHED DATA. OTHER SAMPLES WERE DATED AS PART OF THIS WORK AND SHOWN IN TABLE S3.

TABLE S2: INVERSE MONTE CARLO MODELS RECONSTRUCTED THE RELATIVE CONTRIBUTION TO CLP.

	Central-western CLP		**Eastern CLP**		**Northeastern CLP**	
	Contribution (%)	Standard deviation (%)	Contribution (%)	Standard deviation (%)	Contribution (%)	Standard deviation (%)
HS+Qilian	73.57	11.3	10.72	9.01	1.4	1.89
XNB	8.01	7.27	4.08	3.74	1.9	2.86
MYR+EMU	2.23	1.81	14.04	4.62	91.07	4.31
WMU+UYR	8.65	7.66	52.28	14.66	2.21	2.79
QB	4.26	4.25	7.41	6.39	1.6	1.8
Desert	3.28	3.11	11.47	5.68	1.82	1.98

TABLE S3: U-PB ZIRCON ANALYTICAL DATA FOR THE LEDU AND JIAXIAN LOESS SITES PRESENTED IN THIS STUDY.

TABLE S4: U-PB ZIRCON DATA FOR ALL LOESS SITES AND POTENTIAL SOURCES PRESENTED IN THIS STUDY.

REFERENCES CITED

Andersen, T., 2002, Correction of common lead in U–Pb analyses that do not report 204Pb: Chemical Geology, v. 192, no. 1-2, p. 59-79, doi:10.1016/s0009-2541(02)00195-x.

Bird, A., et al., 2015, Quaternary dust source variation across the Chinese Loess Plateau: Palaeogeography Palaeoclimatology Palaeoecology, v. 435, p. 254-264, doi:10.1016/j.palaeo.2015.06.024.

Black, L. P., et al., 2004, Improved (206)Pb/(238)U microprobe geochronology by the monitoring of a trace-element-related matrix effect; SHRIMP, ID-TIMS, ELA-ICP-MS and oxygen isotope documentation for a series of zircon standards: Chemical Geology, v. 205, no. 1-2, p. 115-140, doi:10.1016/j.chemgeo.2004.01.003.

Black, L. P., Kamo, S. L., Williams, I. S., Mundil, R., Davis, D. W., Korsch, R. J., and Foudoulis, C., 2003, The application of SHRIMP to Phanerozoic geochronology; a critical appraisal of four zircon standards: Chemical Geology, v. 200, no. 1-2, p. 171-188, doi:10.1016/S0009-2541(03)00166-9.

Botev, Z. I., Grotowski, J. F., and Kroese, D. P., 2010, Kernel Density Estimation Via Diffusion: Annals of Statistics, v. 38, no. 5, p. 2916-2957, doi:10.1214/10-Aos799.

Brandon, M. T., 1996, Probability density plot for fission-track grain-age samples: Radiation Measurements, v. 26, no. 5, p. 663-676, doi:Doi 10.1016/S1350-4487(97)82880-6.

Che, X. D., and Li, G. J., 2013, Binary sources of loess on the Chinese Loess Plateau revealed by U-Pb ages of zircon: Quaternary Research, v. 80, no. 3, p. 545-551, doi:10.1016/j.yqres.2013.05.007.

Chen, F., Chen, S., Zhang, X., Chen, J., Wang, X., Gowan, E. J., Qiang, M., Dong, G., Wang, Z., Li, Y., Xu, Q., Xu, Y., Smol, J. P., and Liu, J., 2020, Asian dust-storm activity dominated by Chinese dynasty changes since 2000 BP: Nat Commun, v. 11, no. 1, p. 992, doi:10.1038/s41467-020-14765-4.

Fenn, K., Stevens, T., Bird, A., Limonta, M., Rittner, M., Vermeesch, P., Ando, S., Garzanti, E., Lu, H. Y., Zhang, H. Z., and Lin, Z., 2018, Insights into the provenance of the Chinese Loess Plateau from joint zircon U-Pb and garnet geochemical analysis of last glacial loess: Quaternary Research, v. 89, no. 3, p. 645-659, doi:10.1017/qua.2017.86.

Gehrels, G. E., Valencia, V. A., and Ruiz, J., 2008, Enhanced precision, accuracy, efficiency, and spatial resolution of U-Pb ages by laser ablation-multicollector-inductively coupled plasma-mass spectrometry: Geochemistry Geophysics Geosystems, v. 9, doi:10.1029/2007gc001805.

Jackson, S. E., Pearson, N. J., Griffin, W. L., and Belousova, E. A., 2004, The application of laser ablation-inductively coupled plasma-mass spectrometry to in situ U-Pb zircon geochronology: Chemical Geology, v. 211, no. 1-2, p. 47-69, doi:10.1016/j.chemgeo.2004.06.017.

Kuiper, N. H., 1960, Tests concerning random points on a circle: Indagationes Mathematicae (Proceedings), v. 63, p. 38-47, doi:10.1016/s1385-7258(60)50006-0.

Li, G. Q., et al., 2020, Paleoclimatic changes and modulation of East Asian summer monsoon by high-latitude forcing over the last 130,000 years as revealed by independently dated loess-paleosol sequences on the NE Tibetan Plateau:

Quaternary Science Reviews, v. 237, doi:10.1016/j.quascirev.2020.106283.

Licht, A., Dupont-Nivet, G., Pullen, A., Kapp, P., Abels, H. A., Lai, Z., Guo, Z., Abell, J., and Giesler, D., 2016a, Resilience of the Asian atmospheric circulation shown by Paleogene dust provenance: Nat Commun, v. 7, p. 12390, doi:10.1038/ncomms12390.

Licht, A., Pullen, A., Kapp, P., Abell, J., and Giesler, N., 2016b, Eolian cannibalism: Reworked loess and fluvial sediment as the main sources of the Chinese Loess Plateau: Geological Society of America Bulletin, v. 128, no. 5-6, p. 944-956, doi:10.1130/B31375.1.

Nie, J., et al., 2015, Loess Plateau storage of Northeastern Tibetan Plateau-derived Yellow River sediment: Nat Commun, v. 6, p. 8511, doi:10.1038/ncomms9511.

Nie, J. S., Pullen, A., Garzione, C. N., Peng, W. B., and Wang, Z., 2018, Pre-Quaternary decoupling between Asian aridification and high dust accumulation rates: Science Advances, v. 4, no. 2, doi:10.1126/sciadv.aao6977.

Pearce, N. J. G., Perkins, W. T., Westgate, J. A., Gorton, M. P., Jackson, S. E., Neal, C. R., and Chenery, S. P., 1997, A compilation of new and published major and trace element data for NIST SRM 610 and NIST SRM 612 glass reference materials: Geostandards Newsletter-the Journal of Geostandards and Geoanalysis, v. 21, no. 1, p. 115-144, doi:DOI 10.1111/j.1751-908X.1997.tb00538.x.

Pullen, A., Ibáñez-Mejía, M., Gehrels, G. E., Ibáñez-Mejía, J. C., and Pecha, M., 2014, What happens when n= 1000? Creating large-n geochronological datasets with

LA-ICP-MS for geologic investigations: Journal of Analytical Atomic Spectrometry, v. 29, no. 6, p. 971-980.

Pullen, A., Ibáñez-Mejia, M., Gehrels, G. E., Giesler, D., and Pecha, M., 2018, Optimization of a laser ablation–single collector–inductively coupled plasma–mass spectrometer (Thermo Element 2) for accurate, precise, and efficient zircon U-Th-Pb geochronology: Geochemistry, Geophysics, Geosystems.

Pullen, A., Kapp, P., McCallister, A. T., Chang, H., Gehrels, G. E., Garzione, C. N., Heermance, R. V., and Ding, L., 2011, Qaidam Basin and northern Tibetan Plateau as dust sources for the Chinese Loess Plateau and paleoclimatic implications: Geology, v. 39, no. 11, p. 1031-1034, doi:10.1130/G32296.1.

Qiang, X. K., Li, Z. X., Powell, C. M., and Zheng, H. B., 2001, Magnetostratigraphic record of the Late Miocene onset of the East Asian monsoon, and Pliocene uplift of northern Tibet: Earth and Planetary Science Letters, v. 187, no. 1-2, p. 83-93, doi:Doi 10.1016/S0012-821x(01)00281-3.

Saylor, J. E., Jordan, J. C., Sundell, K. E., Wang, X. M., Wang, S. Q., and Deng, T., 2018, Topographic growth of the Jishi Shan and its impact on basin and hydrology evolution, NE Tibetan Plateau: Basin Research, v. 30, no. 3, p. 544-563, doi:10.1111/bre.12264.

Stevens, T., Carter, A., Watson, T., Vermeesch, P., Andò, S., Bird, A., Lu, H., Garzanti, E., Cottam, M., and Sevastjanova, I., 2013, Genetic linkage between the Yellow River, the Mu Us desert and the Chinese loess plateau: Quaternary Science Reviews, v. 78, p. 355-368.

Stevens, T., Palk, C., Carter, A., Lu, H. Y., and Clift, P. D., 2010, Assessing the provenance of loess and desert sediments in northern China using U-Pb dating and morphology of detrital zircons: Geological Society of America Bulletin, v. 122, no. 7-8, p. 1331-1344, doi:10.1130/B30102.1.

Sundell, K. E., and Saylor, J. E., 2017, Unmixing detrital geochronology age distributions: Geochemistry Geophysics Geosystems, v. 18, no. 8, p. 2872-2886, doi:10.1002/2016GC006774.

Vermeesch, P., 2012, On the visualisation of detrital age distributions: Chemical Geology, v. 312, p. 190-194, doi:10.1016/j.chemgeo.2012.04.021.

Vermeesch, P., 2013, Multi-sample comparison of detrital age distributions: Chemical Geology, v. 341, p. 140-146, doi:10.1016/j.chemgeo.2013.01.010.

Vermeesch, P., 2018, Dissimilarity measures in detrital geochronology: Earth-Science Reviews, v. 178, p. 310-321, doi:10.1016/j.earscirev.2017.11.027.

Wang, Z., Nie, J. S., Wang, J. P., Zhang, H. B., Peng, W. B., Garzanti, E., Hu, X. F., Stevens, T., Pfaff, K., and Pan, B. T., 2019, Testing Contrasting Models of the Formation of the Upper Yellow River Using Heavy-Mineral Data From the Yinchuan Basin Drill Cores: Geophysical Research Letters, v. 46, no. 17-18, p. 10338-10345, doi:10.1029/2019gl084179.

Wiedenbeck, M., Alle, P., Corfu, F., Griffin, W. L., Meier, M., Oberli, F., Vonquadt, A., Roddick, J. C., and Speigel, W., 1995, 3 Natural Zircon Standards for U-Th-Pb, Lu-Hf, Trace-Element and Ree Analyses: Geostandards Newsletter, v. 19, no. 1, p. 1-23, doi:DOI 10.1111/j.1751-908X.1995.tb00147.x.

Xiao, G. Q., Zong, K. Q., Li, G. J., Hu, Z. C., Dupont-Nivet, G., Peng, S. Z., and Zhang, K. X., 2012, Spatial and glacial-interglacial variations in provenance of the Chinese Loess Plateau: Geophysical Research Letters, v. 39, p. 6, doi:10.1029/2012gl053304.

Xiong, J. G., Zhang, H. P., Zhao, X. D., Liu, Q. R., Li, Y. L., and Zhang, P. Z., 2021, Origin of the youngest Cenozoic aeolian deposits in the southeastern Chinese Loess Plateau: Palaeogeography Palaeoclimatology Palaeoecology, v. 561, p. 110080, doi:10.1016/j.palaeo.2020.110080.

Zhang, H. Z., Lu, H. Y., Stevens, T., Feng, H., Fu, Y., Geng, J. Y., and Wang, H. L., 2018, Expansion of Dust Provenance and Aridification of Asia Since similar to 7.2 Ma Revealed by Detrital Zircon U-Pb Dating: Geophysical Research Letters, v. 45, no. 24, p. 13437-13448, doi:10.1029/2018gl079888.

Zhang, H. Z., et al., 2016, Quantitative estimation of the contribution of dust sources to Chinese loess using detrital zircon U-Pb age patterns: Journal of Geophysical Research-Earth Surface, v. 121, no. 11, p. 2085-2099, doi:10.1002/2016jf003936.

Zhang, J., Wang, Y. N., Zhang, B. H., and Zhang, Y. P., 2016, Tectonics of the Xining Basin in NW China and its implications for the evolution of the NE Qinghai-Tibetan Plateau: Basin Research, v. 28, no. 2, p. 159-182, doi:10.1111/bre.12104.

Zhang, X. Y., He, M. Y., Wang, B., Clift, P. D., Rits, D. S., Zheng, Y., and Zheng, H. B., 2019, Provenance evolution of the northern Weihe Basin as an indicator of environmental changes during the Quaternary: Geological Magazine, v. 156, no.

11, p. 1915-1923, doi:10.1017/S0016756819000244.